Development of a Truck-Mounted Arc-Scanning Synthetic Aperture Radar

Hoonyol Lee, *Senior Member, IEEE*, Jae-Hee Lee, *Student Member, IEEE*, Kwang-Eun Kim, *Member, IEEE*, Nak-Hoon Sung, and Seong-Jun Cho

***Abstract*—This paper presents the development of a ground-based arc-scanning synthetic aperture radar (ArcSAR) system mounted on a truck. ArcSAR formulates synthetic aperture by a horizontal circular motion of antennas attached at the end of an extendable boom. The ArcSAR system is designed to operate in two different imaging modes: the *spot mode* and the *scan mode*. The *spot mode* obtains a high-resolution image by fixing the view angle of antennas toward a target. The *scan mode* obtains wider image coverage with a reduced resolution by fixing the antennas relative to the boom. Different SAR focusing algorithms were implemented for the accuracy and efficiency of image processing: the time domain algorithm for the *spot mode* and the range Doppler algorithm for the *scan mode*. An exemplary X-band ArcSAR *spot mode* image, obtained with a 180° scanning of 4-m boom, has an azimuth resolution of 0.07°, which is equivalent to the 12.6-m linear scanning of a conventional ground-based SAR system. An ArcSAR *scan mode* image was successfully obtained as well, covering a 350° image area at an azimuth resolution of 1.07°, which is 11 times better than that of arc-scanning real aperture radar that would have 11.84° azimuth resolution.**

***Index Terms*—Arc-scanning synthetic aperture radar (ArcSAR), range Doppler algorithm, SAR, scan mode, spot mode, time domain algorithm.**

I. Introduction

GROUND-based synthetic aperture radar (GB-SAR) is an imaging radar installed and operated on the ground to obtain high-resolution 2-D image of a scene by forming synthetic aperture with the precise control of antenna position. The GB-SAR systems have actively been developed and tested recently not just as a tool for ground calibration and concept design of innovative satellite SAR systems but also as a system with its own merit of accuracy and repeatability for regional applications [1]–[8]. GB-SAR acquires synthetic aperture by the change of antenna locations with a combination of stepping motor and guided rails [9]. Image focusing can be performed accurately because there is no need of estimating Doppler parameters. If the system is designed not to include motion in transmitting and receiving microwave signal, Doppler centroid is always zero. Doppler rate or even higher order terms of Doppler parameters are exactly known by the stationary radar-target geometry [10]. Even though coherent integration length is limited by the physical length of the rail, GB-SAR can provide continuous data acquisition at a fixed location with great repeatability suitable for various applications such as regional mapping and interferometric SAR detection of surface deformation.

To improve rapid-response capability of GB-SAR, mobility of the system could be increased by mounting the system on a vehicle. However, the scan length is limited by the maximum length of the rail that a vehicle can hold. Therefore, we developed a new ground-based arc-scanning SAR (ArcSAR) system mounted on a truck, with the antenna looking outside of the circular aperture. The idea came from the expectation that a circular arc scanning of antenna with a boom mountable to a truck would increase the Doppler rate, thus resulting in better resolution than a linear scanning with a rail of the same length.

Previous development of systems obtaining synthetic aperture by circular motion can be found in various cases such as airborne circular SAR systems [11]–[13], ground-based circular SAR systems [14]–[19], and geostationary circular SAR [20]. In particular, Rudolf *et al.* [15] had very similar idea to ours in that it was a ground-based system with a target outside of the circular aperture. However, the motion was in the vertical direction to have height resolution of a target, while our system rotates horizontally to map a swath of area with additional resolution in the horizontal direction. Horizontally arc-scanning GB-SAR systems have also been developed so far in L-band [17] and Ka-band [18], which have demonstrated its imaging capability in relatively short range of tens of meters. We further develop the system into two imaging modes—the *spot mode* and the *scan mode*—to compromise between image swath, maximum range, and resolution of the system.

This paper reports the development of the ArcSAR system mounted on a truck. The description of system concept, components, and design is presented in Section II. Based on the geometry similar to the polar format algorithm and considering the processing costs, the time domain algorithm is formulated for the *spot mode* in Section III, while the range Doppler algorithm is used for the *scan mode* in Section IV. The results of the outdoor experiments and the analysis of resolutions are presented in Section V, followed by the concluding remarks in Section VI.

Manuscript received January 5, 2013; revised March 17, 2013; accepted May 21, 2013. Date of publication July 3, 2013; date of current version February 27, 2014. This work was supported by Grant 07KLSGC03 from the Cutting-edge Urban Development—Korean Land Spatialization Research Project funded by the Ministry of Land, Transport and Maritime Affairs of the Korean Government.

H. Lee is with the Department of Geophysics, Kangwon National University, Chuncheon 200-701, Korea (e-mail: hoonyol@kangwon.ac.kr).

J.-H. Lee is with the Department of Geophysics, Kangwon National University, Chuncheon 200-701, Korea, and also with the Korea Institute of Geoscience and Mineral Resources, Daejeon 305-350, Korea.

K.-E. Kim, N.-H. Sung, and S.-J. Cho are with the Korea Institute of Geoscience and Mineral Resources, Daejeon 305-350, Korea.

Color versions of one or more of the figures in this paper are available online at http://ieeexplore.ieee.org.

Digital Object Identifier 10.1109/TGRS.2013.2265700

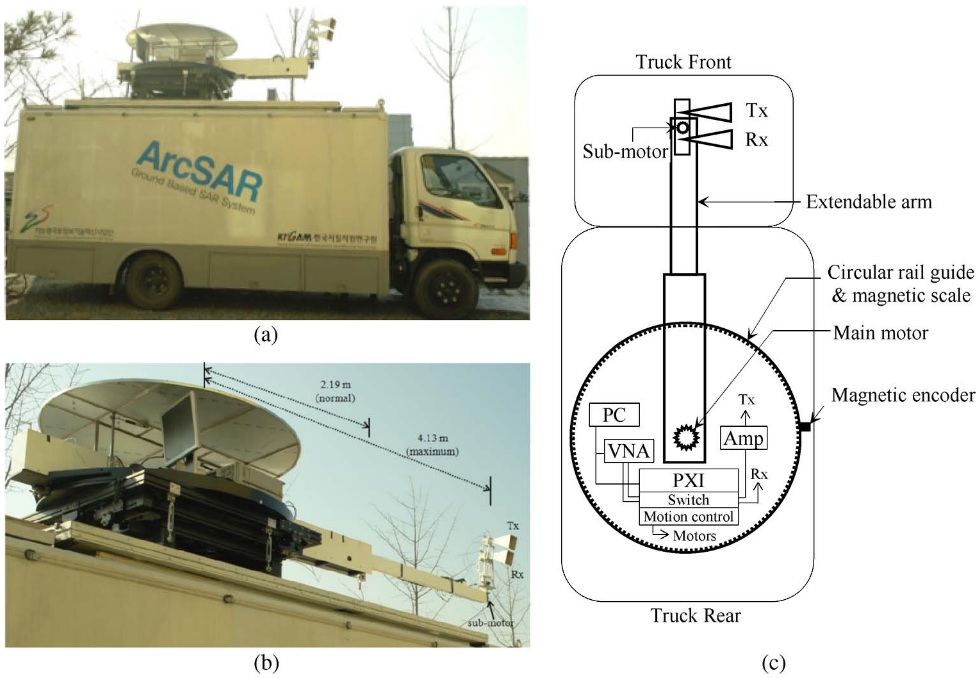

Fig. 1. ArcSAR system mounted on a truck. (a) Side view. (b) Oblique view. (c) Schematic diagram in top view.

II. ArcSAR System

Fig. 1 shows the ArcSAR system mounted on a truck. The ArcSAR system acquires images by transmitting and receiving microwave signals through the antennas attached at the end of an extendable boom. The boom is mounted on top of a platform that rotates along a circular rail guide by the main motor. The length of the boom is 2.19 m and is extendable to 4.19 m. Any kind of antenna can be attached to the boom as long as its weight and shape do not harm the stability of the system. We used two identical dual-polarization square-horn X-band antennas for Tx and Rx. An orthogonal mode transducer is attached to each antenna for the selection of vertical and horizontal polarizations. The antenna mount is designed to align the Tx and Rx antennas either in horizontal or vertical direction. The horizontal look direction of the antennas can be adjusted automatically by the submotor. The main motor is a stepped motor that has the resolution of 2.4×10^{-4} °/step. An additional magnetic scale and an encoder were implemented to monitor the position of the boom with 10-μm accuracy. The submotor also shows very accurate positioning capability with a 3.6×10^{-2} °/step resolution. In order to record the circumstances during the data acquisition, an optical camera system was implemented at the antenna mount to provide images from the antenna view point (not shown in Fig. 1). The whole system is stored inside the cargo bay of the truck during transportation and is elevated out of the truck by a motorized jack system.

The RF part of the system is mainly composed of a vector network analyzer (Agilent E8362B), a microwave amplifier, a microwave switch module (NI PXI-2599), and a computer inside the NI PXI-1031 chassis. A stepped-frequency microwave signal is generated from the vector network analyzer. The signal is sent to the selected polarization of the Tx antenna via the microwave switch module. The signal returned from targets is collected by the Rx antenna with a particular polarization selected by the switch. The data are then stored to the hard disk of the computer. The system has different geometry from conventional linear-scanning GB-SAR systems and requires new focusing algorithms to produce images out of the scanned data.

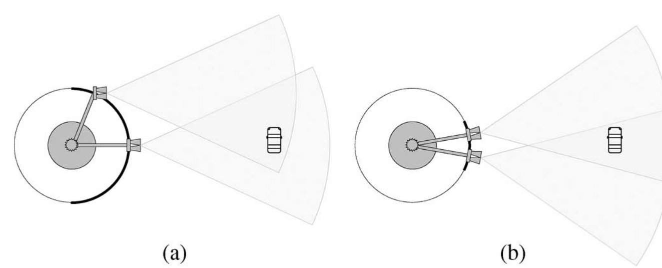

Fig. 2. Schematic diagram of the two scanning modes of ArcSAR (top view). (a) *Spot mode*. (b) *Scan mode*. Thick arcs are the coherent integration arc for each target.

ArcSAR can operate in two different scanning modes: the *spot mode* and the *scan mode* (Fig. 2). In the *spot mode*, the antennas attached to the end of the boom can be rotated in azimuth direction by the submotor, enabling continuous look to the designated target area [Fig. 2(a)]. Coherent integration arc is as long as the half-circle of the scanning boom to produce higher resolution than the linear-scanning GB-SAR systems with the same length of boom [9], [10]. In the *scan mode*, the antennas are fixed relative to the boom during the scan with no submotor action involved [Fig. 2(b)]. The data can be obtained continuously during the rotation so that it can image the whole azimuth angle (360°) around the system. The coherent integration arc of the *scan mode* is limited to the beamwidth, resulting in lower resolution, but still has advantage in resolution when compared to an arc-scanning real aperture radar (ArcRAR) without SAR focusing.

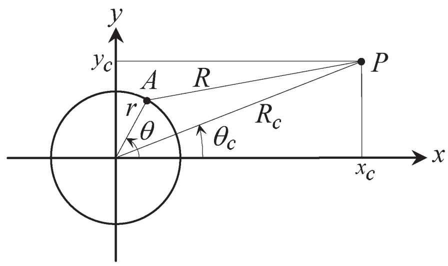

Fig. 3. ArcSAR imaging geometry where the antenna is at a point A and a target is at P (top view).

III. Focusing of ArcSAR Spot Mode

A. Time Domain Algorithm in Polar Coordinates

Consider a point target $P(x_c, y_c)$ in rectangular coordinates as shown in Fig. 3. It can be expressed as $P(R_c, \theta_c)$ in polar coordinates by the following relations [19]:

$$x_c = R_c \cos\theta_c \quad y_c = R_c \sin\theta_c. \tag{1}$$

ArcSAR *spot mode* data are obtained by the rotation of a boom with a length of r and sweeping azimuth swath of θ_s (*coherent integration arc*) from $-\theta_s/2$ to $\theta_s/2$ around the axis fixed at the origin of the polar coordinates. The returned data are base-banded and Hamming-filtered in the range direction. An inverse-FFT is then applied to the data to obtain a range-compressed data. The returned signal from a point target to the antenna at azimuth θ can be expressed by

$$s(\theta|R_c, \theta_c) = e^{-j\frac{4\pi}{\lambda}R(\theta|R_c,\theta_c)}, \quad |\theta| < \theta_s/2 \tag{2}$$

where R is the range from the antenna to the target, given by

$$R(\theta|R_c, \theta_c) = \sqrt{R_c^2 + r^2 - 2R_c r\cos(\theta - \theta_c)}. \tag{3}$$

Range migration for the point target can be performed exactly according to (3) without any approximation. SAR focusing can be formulated by the following correlation:

$$g(\xi|R_c, \theta_c) = \int s(\theta|R_c, \theta_c)h^{-1}(\theta - \xi|R_c, \theta_c)d\theta \tag{4}$$

where $h^{-1}(\theta) = s*(\theta)$. ArcSAR focusing at $P(x_c, y_c)$ can be performed by directly evaluating the aforementioned integral at $\xi = 0$, where the peak value of the aforementioned equation will occur, resulting in

$$g(R_c, \theta_c) = \int s(\theta)s*(\theta)d\theta = \theta_s. \tag{5}$$

Even though evaluating the aforementioned integration for all imaging space is very time-consuming, ArcSAR *spot mode* focusing was performed in the "time domain" as it is accurate and exact with no assumption. However, it is difficult to analyze the resolution of the image theoretically because we cannot evaluate the aforementioned correlation in (4) in a closed form. Therefore, we introduce the deramp-FFT algorithm in polar coordinates in a closed form to evaluate the performance and resolution of the ArcSAR *spot mode*.

B. Image Analysis Using Deramp-FFT Algorithm

The formulation of the deramp-FFT algorithm begins with the Taylor's expansion of (3) at $\theta = 0$ by

$$R(\theta|R_c, \theta_c) = R(0) + R'(0)\theta + \frac{R''(0)}{2!}\theta^2 + \frac{R'''(0)}{3!}\theta^3 + \cdots \tag{6}$$

where

$$R(0) = R_0 = \sqrt{R_c^2 + r^2 - 2R_c r\cos\theta_c} \tag{7}$$

$$R'(0) = -\frac{rR_c\sin\theta_c}{R_0} \tag{8}$$

$$R''(0) = \frac{R_c r\cos\theta_c}{R_0} - \frac{R_c^2 r^2\sin^2\theta_c}{R_0^3}, \quad \text{and so on.} \tag{9}$$

SAR focusing can be performed by multiplying the received signal with a deramp function followed by Fourier transformation in azimuth direction

$$g(\xi|R_c, \theta_c) = \int s(\theta)h^{-1}(\theta)e^{-j2\pi\xi\theta}d\theta. \tag{10}$$

The deramp function is chosen to include the terms higher and equal to the second order of (6) as in the following:

$$h^{-1}(\theta|R_c, \theta_c) = e^{j\frac{4\pi}{\lambda}\left[R''(0)\theta^2/2! + R'''(0)\theta^3/3! + \cdots\cdots\right]} \tag{11}$$

so that the integrand in (10) is reduced to the following simplified form:

$$g(\xi|R_c, \theta_c) = \int_{-\theta_s/2}^{\theta_s/2} e^{-j\frac{4\pi}{\lambda}[R(0) + R'(0)\theta]}e^{-j2\pi\xi\theta}d\theta. \tag{12}$$

Analytic evaluation of (12) gives the following focused image:

$$g(\xi|R_c, \theta_c) = \theta_s e^{-j\frac{4\pi}{\lambda}R_0}\text{sinc}\left[\pi\theta_s\left(\xi - \frac{2R_c r\sin\theta_c}{\lambda R_0}\right)\right]. \tag{13}$$

The focused image has the maximum amplitude of θ_s in ξ-space at

$$\xi = \frac{2R_c r\sin\theta_c}{\lambda R_0}. \tag{14}$$

The phase value of the focused image is $\phi = -4\pi R_0/\lambda$, which is a measure of the range from the origin at $(r, 0)$ in polar coordinates to the target, enabling its use for SAR interferometry.

The focused image in ξ-space can be geometrically transformed into the polar coordinates or the rectangular coordinates by the following equations:

$$\theta_c = \sin^{-1}\left(\frac{\lambda R_0\xi}{2R_c r}\right). \tag{15}$$

The half power of the sinc function (13) gives the definitions of azimuth resolution in various domains such as

$$\delta\xi = 1/\theta_s \tag{16}$$

$$\delta\theta_c = \frac{\lambda}{2r\theta_s}\cdot\frac{R_0}{R_c\cos\theta_c} \approx \frac{\lambda}{2r\theta_s} \text{ (at far range).} \tag{17}$$

The aforementioned three equations indicate that we can expect higher azimuth resolution by enlarging the length of the antenna boom, by increasing the coherent integration arc, or by using a shorter wavelength (higher frequency).

The azimuth angular resolution of a conventional linear-scanning GB-SAR system with a scan-length of L_s is given as [10]

$$\delta\theta_c = \frac{\lambda}{2L_s}. \tag{18}$$

When compared with it, the effect of arc scanning is equivalent to the linear scanning of

$$L_s = r\theta_s. \tag{19}$$

The ArcSAR *spot mode* has the maximum coherent integration arc value of $\theta_s = \pi$ due to the intervention of truck structure. In such case, $L_s = \pi r$, which indicates that the ArcSAR *spot mode* has π times longer synthetic aperture length than a linear-scanning GB-SAR system of which the scan length is r.

The deramp function presented in (11) is a function of azimuth θ_c of the imaging space, which means that the FFT should be performed at each azimuth with a different deramp function. This processing is as time-consuming as the time domain algorithm. In a linear-scanning GB-SAR, the deramp-FFT algorithm can be simplified by approximately choosing a common deramp function irrespective of azimuth as the one at the center azimuth of the image ($\theta_c = 0$) of (11) and (9)

$$\tilde{h}^{-1} = h^{-1}(\theta|R_c, \theta_c = 0). \tag{20}$$

The overall focusing is then simplified by applying FFT in azimuth direction. However, image degradation is expected due to the aforementioned approximation. The degradation was known to be tolerable for a linear-scanning GB-SAR system [10] but not for the ArcSAR *spot mode* which has greater angular diversity of coherent integration arc. Therefore, the deramp-FFT algorithm is used here as a tool to evaluate the image formation of ArcSAR *spot mode* in a closed form, while the actual SAR focusing is done by the time domain algorithm as described previously.

IV. Focusing of ArcSAR Scan Mode

As the *scan mode* obtains data continuously in polar format for the target at $P(x_c, y_c)$ in rectangular coordinates or equivalently $P(R_c, \theta_c)$ in polar coordinates, the range Doppler algorithm in polar format is an efficient way of SAR focusing. After the range compression, the collected signal is represented as

$$s(\theta|R_c, \theta_c) = e^{-j\frac{4\pi}{\lambda}R(\theta|R_c,\theta_c)}, \quad |\theta - \theta_c| < \theta_s/2 = \frac{\lambda}{2L}. \tag{21}$$

The coherent integration arc θ_s for the *scan mode* is limited by the width of the antenna beam. Similarly, we have the range from the antenna to the target as

$$R(\theta|R_c, \theta_c) = \sqrt{R_c^2 + r^2 - 2R_c r\cos(\theta - \theta_c)}. \tag{22}$$

Different from the *spot mode*, we expand the aforementioned equation at the target itself $\theta = \theta_c$ so that

$$R(\theta) = R(\theta_c) + R'(\theta_c)\theta + \frac{R''(\theta_c)}{2!}\theta^2 + \cdots \tag{23}$$

where

$$R(\theta_c) = R_c - r \tag{24}$$
$$R'(\theta_c) = 0 \tag{25}$$
$$R''(\theta_c) = \frac{R_c r}{R(\theta_c)} = \frac{R_c r}{R_c - r}. \tag{26}$$

Using the wavenumber Doppler parameters, we obtain

$$R(\theta) = R(\theta_c) - \frac{\lambda u_{\mathrm{Dc}}}{2}(\theta - \theta_c) - \frac{\lambda u_R}{4}(\theta - \theta_c)^2 + \cdots \tag{27}$$

where u_{Dc} and u_R are the Doppler centroid and the Doppler rate, respectively, given by

$$u_{\mathrm{Dc}} = 0 \tag{28}$$
$$u_R = -\frac{2}{\lambda}\frac{R_c r}{R_c - r}. \tag{29}$$

Ignoring the terms higher than quadratic, the received signal becomes

$$s(\theta|R_c, \theta_c) \simeq e^{-j\frac{4\pi}{\lambda}R(\theta_c)} e^{j2\pi\left[u_{\mathrm{Dc}}(\theta-\theta_c) + u_R(\theta-\theta_c)^2/2\right]}. \tag{30}$$

The signal comprises a linear chirp as a function of azimuth. The matched filter for range Doppler algorithm is defined as

$$h^{-1}(\theta) = e^{-j2\pi\left[u_{\mathrm{Dc}}\theta + u_R\theta^2/2\right]}. \tag{31}$$

The data are compressed in azimuth direction by the following filtering:

$$g(\theta) = \int h^{-1}(\theta' - \theta)s(\theta')d\theta'. \tag{32}$$

The evaluation of the aforementioned integration with the range of θ' to be $[\theta_c - \theta_s/2, \theta_c + \theta_s/2]$ gives

$$g(\theta) = \theta_s \mathrm{sinc}\left[\frac{2\pi R_c r\theta_s}{\lambda(R_c - r)}(\theta - \theta_c)\right] e^{-j\frac{4\pi}{\lambda}(R_c - r)} e^{j2\pi\left[\frac{(\theta-\theta_c)^2}{\lambda(R_c-r)}\right]}. \tag{33}$$

The phase is $\phi = -(4\pi/\lambda)(R_c - r)$ so that the image is from the antenna (not from the center of the arc) to the target. The processed image is in (R, θ) domain and should be transformed into (x, y) space for display by using (1). The aforementioned signal has a maximum value of θ_s at $\theta = \theta_c$. The azimuth angular resolution is defined as

$$\delta\theta = \frac{\lambda(R_c - r)}{2R_c r\theta_s} \approx \frac{\lambda}{2r\theta_s} = \frac{L}{2r} \tag{34}$$

using (21) for coherent integration arc. The aforementioned approximation is valid at large range where $R_c \gg r$. The azimuth resolution of the ArcSAR *scan mode* can be improved by reducing the antenna size or by enlarging the length of the rotational boom, but it is not relevant to the choice of wavenumber λ. Image degradation by ignoring higher terms in (27) is tolerable for ArcSAR *scan mode* because of a shorter coherent integration arc than that of ArcSAR spot mode. This will be shown experimentally in the following section.

TABLE I
PARAMETERS FOR ARCSAR EXPERIMENTS

System Parameters	*Spot Mode*	*Scan Mode*
Acquisition date	20 Oct. 2011	13 Dec. 2011
Location	Eunhasu Park, Sejong	Yeayang-ri, Sejong
Center frequency	9.65 GHz	
Bandwidth	0.3 GHz	
Range resolution	0.5 m	
Number of range samples	801	1601
Maximum range	200 m	400 m
Boom length	4.00 m	
Antenna aperture width	0.15 m	
Antenna gain	21 dBi	
Azimuth beam width (-3dB)	11.84°	
Azimuth sampling interval	0.54°	
Azimuth scan angle	180°	350°
Azimuth resolution	0.07°	1.07°
Azimuth image swath	32°	350°
Scanning Time	14 min	27 min
Focusing Algorithm	Time Domain Algorithm	Range Doppler Algorithm
Polarization	VV	
Tx Power	37 dBm	

V. RESULTS AND DISCUSSIONS

A. Outdoor Experimental Results

Table I shows the parameters for the ArcSAR experiment. The bandwidth is 300 MHz so that the range resolution is 50 cm. The boom length was set to 4 m. Azimuth sampling interval was chosen to be 0.54° as a compromise between azimuth ambiguity and the scan rates. The output power of the Tx signal was 37 dBm, and the polarization is VV. The first experiment on the ArcSAR *spot mode* was conducted on October 20, 2011, at Eunhasu Park, Sejong City, Korea. Fig. 4 shows an image of the ArcSAR *spot mode* and the corresponding optical image of the study area. Azimuth coherent integration arc was 180°, and the corresponding azimuth resolution was 0.07°. Focusing was performed with time domain algorithm in polar coordinates. The azimuth beamwidth of the antenna was 11.84°, while the azimuth image swath was processed to be 32°. The maximum range of the image was 200 m. The three trihedral corner reflectors with 50-cm hypotenuse are clearly seen in the image. Poles of the street lamps along the road and buildings are the major features of strong backscattering in the *spot mode* image.

Fig. 5 shows the ArcSAR *scan mode* image and the corresponding optical image of the study area. The experiment was performed on December 13, 2011, at Yeayang-ri, Sejong City, Korea. The coherent integration arc was the same with the 11.84° of the antenna beamwidth, resulting in the azimuth resolution of 1.07°. The focusing was performed with range Doppler algorithm in polar coordinates as described in the previous section. Azimuth image swath of 350° was obtained with the maximum range of the image of 400 m, leaving the approximately 10° of azimuth gap at the left side of the image. The structures of roads and agricultural houses are clearly imaged. Severe degradation of resolution is seen at far range as a consequence of azimuth angular resolution.

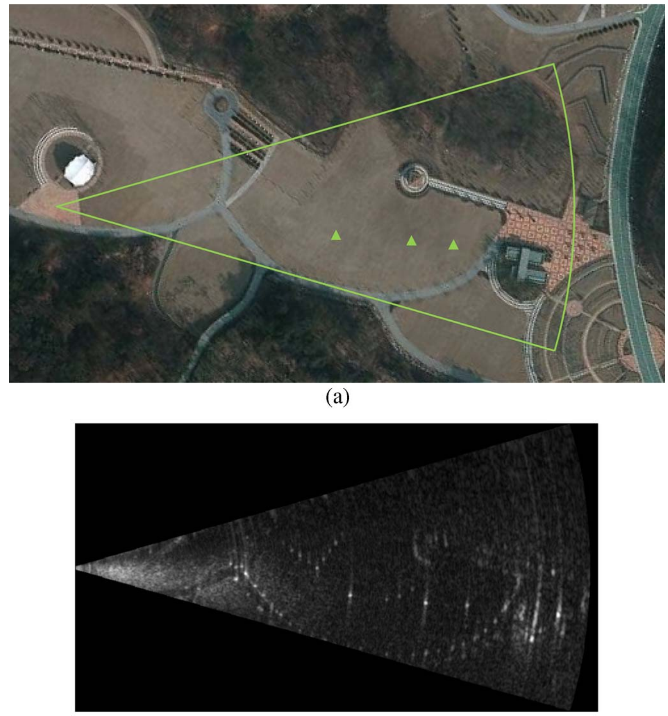

Fig. 4. Example of the ArcSAR *spot mode*. (a) Aerial photograph. (b) ArcSAR *spot mode* image. The triangles in (a) indicate the locations of the corner reflectors. The maximum range is 200 m.

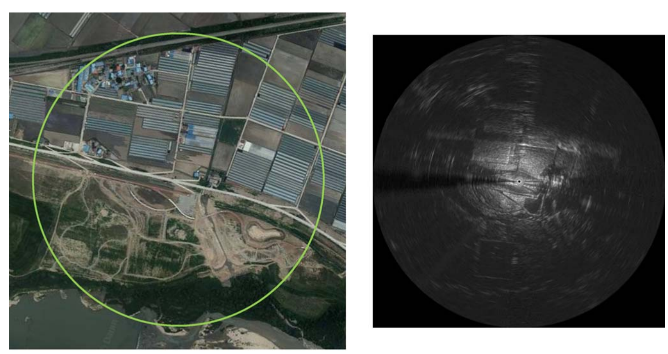

Fig. 5. Example ArcSAR *scan mode* image. (a) Aerial photograph. (b) ArcSAR *scan mode* image. The radius of the circle is 400 m.

B. Comparison of Resolutions

The resolutions of the various imaging modes of the ArcSAR system such as ArcRAR (ArcRAR of ArcSAR system without SAR focusing), ArcSAR *scan mode*, and ArcSAR *spot mode* are compared with a linear-scanning GB-SAR in Table II. Azimuth angular resolutions are shown in numbers in the first column. Here, the X-band system has the wavelength of $\lambda = 0.031$ m, the azimuth antenna width of $L = 0.15$ m, the length of the boom $r = 4$ m, the coherent integration arc of $\theta_s = \pi$ (180°) for the ArcSAR *spot mode*, and the linear-scanning GB-SAR length of $L_s = 4$ m (the same as the boom)

TABLE II

COMPARISON OF AZIMUTH RESOLUTIONS AND THEIR RATIOS BETWEEN THE ARCRAR, THE ARCSAR Scan Mode, THE LINEAR-SCANNING GB-SAR, AND THE ARCSAR Spot Mode. ANALYTICAL FORMULAS ARE SHOWN AT THE LOWER TRIANGLE OF THE TABLE, WHILE NUMERICAL VALUES ARE SHOWN AT THE UPPER PART. NUMERICAL VALUES ARE THE RATIO OF RESOLUTIONS BASED ON AN X-BAND SYSTEM WITH $\lambda = 0.031$ m, $L = 0.15$ m, $r = 4$ m, $L_s = 4$ m (FOR GB-SAR), AND $\theta_s = 180°$ (FOR ARCSAR Spot Mode). THE NUMBER IN PARENTHESIS IN EACH CELL IS THE INVERSE VALUE

Azimuth Resolution: ($\delta\theta$) — degree / radian	ArcRAR: 11.84°	ArcSAR *Scan Mode*: 1.07°	Linear GB-SAR: 0.22°	ArcSAR *Spot Mode*: 0.07°
ArcRAR: $\frac{\lambda}{L}$	1	9.07e-2 (11.0)	1.87e-2 (53.4)	5.98e-3 (167.2)
ArcSAR *Scan mode*: $\frac{L}{2r}$	$\frac{L^2}{2\lambda r}$	1	2.07e-1 (4.8)	6.58e-2 (15.2)
Linear GB-SAR: $\frac{\lambda}{2L_s}$	$\frac{L}{2L_s}$	$\frac{\lambda r}{LL_s}$	1	3.18e-1 (3.14)
ArcSAR *Spot mode*: $\frac{\lambda}{2r\theta_s}$	$\frac{L}{2r\theta_s}$	$\frac{\lambda}{\theta_s L}$	$\frac{L_s}{r\theta_s}$	1

for comparison. Resolutions in formula are shown at the first column of the table. Ratios of azimuth resolutions are depicted in numbers at the upper half triangle while in formula at the lower half triangle. ArcRAR has the poorest resolution because the azimuth resolution is simply the antenna beamwidth

$$\delta\theta = \frac{\lambda}{L} = 0.207 \text{ radian } (= 11.84°). \tag{35}$$

The resolution of the ArcSAR *scan mode* is 1.07°, which was enhanced by 11 times over the ArcRAR. It is 4.8 times lower than the conventional linear GB-SAR (0.22°) but has the advantage of omnidirectional coverage. The ArcSAR *spot mode* has 0.07° of azimuth resolution, which is 3.14 times better than that of the GB-SAR system that has the same length of linear scan with the ArcSAR boom. In other words, the ArcSAR *spot mode* image with a 4-m boom has an azimuth resolution equivalent to the 12.6-m linear scanning of a conventional GB-SAR system. ArcSAR *spot mode* has 15.2 times higher resolution than the ArcSAR *scan mode* and is 167.2 times better than ArcRAR, with a reduced image swath.

VI. CONCLUSION

A truck-mounted ArcSAR system has been constructed and tested successfully by outdoor experiments. Image focusing algorithms for ArcSAR were developed in polar coordinates, which use time domain algorithm for the ArcSAR *spot mode* and range Doppler algorithm for the ArcSAR *scan mode*. Comparisons of image resolutions between various imaging modes of ArcSAR system confirmed the advantage of the high resolution of the ArcSAR *spot mode* and the wide-scanning capability of the ArcSAR *scan mode* over a linear-scanning GB-SAR and the unfocused ArcRAR, respectively. ArcSAR *spot mode* with an extendable boom has the highest azimuth resolution equivalent to π-times of a linear-scanning GB-SAR. ArcSAR *scan mode* has poorer resolution than the ArcSAR *spot mode* and a linear-scanning GB-SAR but has omnidirectional coverage with still 11 times higher resolution than that of ArcRAR (an unfocused ArcSAR image mode). Mounted on a truck, the system is expected to provide a rapid response tool to various applications such as regional mapping and environmental hazard monitoring.

REFERENCES

[1] D. Tarchi, H. Rudolf, M. Pieraccini, M. , and C. Atzeni, "Remote monitoring of buildings using a ground-based SAR: Application to cultural heritage survey," *Int. J. Remote Sens.*, vol. 21, no. 18, pp. 3545–3551, Jan. 2000.

[2] J. C. Bennett, K. Morrison, A. Race, G. Cookmartin, and S. Quegan, "The UK NERC fully portable polarimetric ground-based synthetic aperture radar (GB-SAR)," in *Proc. IEEE IGARSS*, Jul. 24–28, 2000, vol. 5, pp. 2313–2315.

[3] D. Leva, G. Nico, D. Tarchi, J. Fortuny-Guasch, and A. J. Sieber, "Temporal analysis of a landslide by means of a ground-based SAR interferometer," *IEEE Trans. Geosci. Remote Sens.*, vol. 41, no. 4, pp. 745–757, Apr. 2003.

[4] D. Tarchi, N. Casagli, R. Fanti, D. Leva, G. Luzi, A. Pasuto, M. Pieraccini, and S. Silvano, "Landslide monitoring by using ground-based SAR interferometry: An example of application to the Tessina landslide in Italy," *Eng. Geol.*, vol. 68, no. 1/2, pp. 15–30, Feb. 2003.

[5] G. Luzi, M. Pieraccini, D. Mecatti, L. Noferini, G. Guidi, F. Moia, and C. Atzeni, "Ground-based radar interferometry for landslides monitoring: Atmospheric and instrumental decorrelation sources on experimental data," *IEEE Trans. Geosci. Remote Sens.*, vol. 42, no. 11, pp. 2454–2466, Nov. 2004.

[6] Z. S. Zhou, W. M. Boerner, and M. Sato, "Development of a ground-based polarimetric broadband SAR system for noninvasive ground-truth validation in vegetation monitoring," *IEEE Trans. Geosci. Remote Sens.*, vol. 42, no. 9, pp. 1803–1810, Sep. 2004.

[7] G. Nico, D. Leva, J. Fortuny-Guasch, G. Antonello, and D. Tarchi, "Generation of digital terrain models with a ground-based SAR system," *IEEE Trans. Geosci. Remote Sens.*, vol. 43, no. 1, pp. 45–49, Jan. 2005.

[8] L. Noferini, M. Pieraccini, D. Mecatti, G. Luzi, A. C. Atzeni, and M. Broccolato, "Permanent scatterers analysis for atmospheric correction in ground-based SAR interferometry," *IEEE Trans. Geosci. Remote Sens.*, vol. 43, no. 7, pp. 1459–1471, Jul. 2005.

[9] H. Lee, S. J. Cho, N. H. Sung, and J. H. Kim, "Development of a GB-SAR (I): System configuration and interferometry," *Korean J. Remote Sens.*, vol. 23, no. 4, pp. 237–245, 2007.

[10] H. Lee, S. J. Cho, N. H. Sung, and J. H. Kim, "Development of a GB-SAR (II): Focusing algorithm," *Korean J. Remote Sens.*, vol. 23, no. 4, pp. 247–256, 2007.

[11] M. Soumekh, "Reconnaissance with slant plane circular SAR imaging," *IEEE Trans. Image Process.*, vol. 5, no. 8, pp. 1252–1265, Aug. 1996.

[12] Y. Li and D. Zhu, "The geometric-distortion correction algorithm for circular-scanning SAR imaging," *IEEE Geosci. Remote Sens. Lett.*, vol. 7, no. 2, pp. 376–380, Apr. 2010.

[13] Y. Lin, W. Hong, W. Tan, Y. Wang, and Y. Wu, "Interferometric circular SAR method for three-dimensional imaging," *IEEE Geosci. Remote Sens. Lett.*, vol. 8, no. 6, pp. 1026–1030, Nov. 2011.

[14] A. Broquetas, R. De Porrata, L. Sagués, X. Fàbregas, and L. Jofre, "Circular synthetic aperture radar (C-SAR) system for ground-based applications," *Electron. Lett.*, vol. 33, no. 11, pp. 988–989, May 1997.

[15] H. Rudolf, D. Leva, D. Tarchi, and A. J. Sieber, "A parallelogram shaped arm for improving circular SARs," in *Proc. IEEE IGARSS*, 1999, vol. 1, pp. 553–555.

[16] M. Bara, L. Sagués, F. Paniagua, A. Broquetas, and X. Fàbregas, "High-speed focusing algorithm for circular synthetic aperture radar (C-SAR)," *Electron Lett.*, vol. 36, no. 9, pp. 828–830, Apr. 2000.

[17] D. S. Garmatyuk and R. M. Narayanan, "Ultra-wideband continuous-wave random noise Arc-SAR," *IEEE Trans. Geosci. Remote Sens.*, vol. 40, no. 12, pp. 2543–2552, Dec. 2002.

[18] J. D. Taylor, *Ultrawideband Radar: Applications and Design*. New York, NY, USA: CRC Press, ch. 6, pp. 216–218.

[19] H. Lee, S. J. Cho, and K. E. Kim, "A ground-based arc-scanning synthetic aperture radar (ArcSAR) system and focusing algorithms," in *Proc. IEEE IGARSS*, 2010, pp. 3490–3493.

[20] X. Wang, M. Xiang, and M. Zhu, "Interferometric estimation of three-dimensional surface deformation using geosynchronous circular SAR," *IEEE Trans. Aerosp. Electron. Syst.*, vol. 48, no. 2, pp. 1619–1635, Apr. 2012.

Hoonyol Lee (S'99–M'01–SM'11) was born in Kwangju, Korea, in 1969. He received the B.S. degree in geology and the M.S. degree in geophysics from Seoul National University, Seoul, Korea, in 1995 and 1997, respectively, and the Ph.D. degree in radar remote sensing from the Department of Earth Sciences and Engineering, Imperial College London, University of London, London, U.K., in 2001.

From 2001 to 2003, he was a Postdoctoral Research Associate with Imperial College London. From 2003 to 2004, he was a Senior Researcher with the Korea Institute of Geoscience and Mineral Resources (KIGAM), Daejeon, Korea. Since 2004, he has been with the Department of Geophysics, Kangwon National University, Chuncheon, Korea, where he is currently an Associate Professor. From August 2008 to July 2009, he was a Visiting Scholar with the Department of Geological Sciences, University of Oregon, Eugene, OR, USA. His research interests include synthetic aperture radar (SAR), interferometry, and polarimetry. He developed an educational SAR processor, a SAR ocean processor, polarimetric scatterometer systems, and ground-based SAR systems.

Prof. Lee was supported by the Korean Ministry of Education Scholarship, the Overseas Research Student Award from the Committee of Vice-Chancellor and Principals, U.K., and the Chevening Scholarship from the British Embassy in Korea for his Ph.D. study. He was awarded the Interactive Session Prize Paper Award at the 1999 IEEE International Geoscience and Remote Sensing Symposium (IGARSS'99), Hamburg, Germany. In 2008, he received the Best Paper Award from the *Korean Journal of Remote Sensing*. He is a senior member of the IEEE Geoscience and Remote Sensing Society and a member of the American Geophysical Union. From 2011 to 2013, he served as the Editor-in-Chief of the *Korean Journal of Remote Sensing*.

Jae-Hee Lee (S'08) was born in Wonju, Korea, in March 1982. He received the B.S. and M.S. degrees in geophysics from Kangwon National University, Chuncheon, Korea, in 2008 and 2010, respectively.

From 2008 to 2010, he was a research student with the Korea Institute of Geoscience and Mineral Resources (KIGAM), Daejeon, Korea, where he was a Contract Researcher from 2010 to 2012. His research interests include ground-based synthetic aperture radar and arc-scanning synthetic aperture radar systems for detailed change detection through atmospheric correction.

Mr. Lee received Student Paper Awards at the Korea Remote Sensing Symposia in 2009.

Kwang-Eun Kim (M'03) received the B.S. degree in mineral engineering, the M.S. degree in exploration geophysics, and the Ph.D. degree in remote sensing from Seoul National University, Seoul, Korea, in 1985, 1987, and 1993, respectively. His Ph.D. dissertation was "Atmospheric correction using covariance of data with two different scan angles in airborne thermal infrared remote sensing."

He is currently a Principal Researcher with the Mineral Resources Research Division, Korea Institute of Geoscience and Mineral Resources (KIGAM), Daejeon, Korea. He is also an Adjunct Professor with the Department of Energy Resources Engineering, Seoul National University. He further studied geologic remote sensing and geospatial analysis techniques as a Visiting Scientist at Geological Survey of Canada in 1997–1998. He developed a software package for remote sensing image data processing and analysis called PG-STEAMER while he was a CTO of Pixoneer Geomatics, Inc., in 1998–2004. He published a few tens of research papers at various international and Korean journals in the field of remote sensing.

Dr. Kim has been the Vice-President of the Korean Society of Remote Sensing since 2011. He received the Best Paper Award from the *Korean Journal of Remote Sensing* in 2011.

Nak-Hoon Sung was born in Anyang, Korea, in September 1952. He received the B.S. degree from Seoul National University of Science and Technology, Seoul, Korea, in 1985, the M.S. degree from Yonsei University, Seoul, in 1987, and the Ph.D. degree in geophysical exploration from Chonbuk National University, Jeonju, Korea, in 2010, with the dissertation "Measurement System and Application of Database for Rock Physical Properties."

He is currently with the Department of Exploration Geophysics and Mining Engineering, Korea Institute of Geoscience and Mineral Resources (KIGAM), Daejeon, Korea.

Seong-Jun Cho received the B.Eng. degree in petroleum and mineral resources engineering, the M.Eng. degree, and the Ph.D. degree in applied geophysics from the National Seoul University, Seoul, Korea, in 1991, 1993, and 2000, respectively.

From 2004 to 2005, he was a Visiting Researcher with the Center for Northeast Asian Studies, Tohoku University, Sendai, Japan. He is currently a Principal Geophysicist with the Department of Exploration Geophysics and Mining Engineering, Korea Institute of Geoscience and Mineral Resources (KIGAM), Daejeon, Korea. He has over 19 years of experience in the research for the development of geophysical exploration technologies. His current interests include borehole radar and ground-penetrating radar imaging, low-frequency EM modeling and inversion, and geophysical measurement systems.